

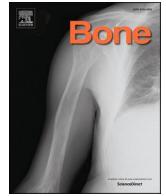


Title	RANKL-derived peptide MHP1-AcN attenuates ovariectomy-induced osteoporosis by targeting RANK and TNFR1 in mice
Author(s)	Kurihara, Takuya; Shimamura, Munehisa; Etani, Yuki et al.
Citation	Bone. 2025, 194, p. 117440
Version Type	VoR
URL	https://hdl.handle.net/11094/100972
rights	This article is licensed under a Creative Commons Attribution-NonCommercial-NoDerivatives 4.0 International License.
Note	

The University of Osaka Institutional Knowledge Archive : OUKA

<https://ir.library.osaka-u.ac.jp/>

The University of Osaka



Full Length Article



RANKL-derived peptide MHP1-AcN attenuates ovariectomy-induced osteoporosis by targeting RANK and TNFR1 in mice

Takuya Kurihara ^a, Munehisa Shimamura ^b, Yuki Etani ^{a,c}, Takaaki Noguchi ^a, Yuji Fukuda ^a, Nagahiro Ochiai ^d, Atsushi Goshima ^e, Taihei Miura ^f, Makoto Hirao ^g, Atsushi Sugimoto ^a, Nan Ju ^b, Satoshi Yamakawa ^h, Takashi Kanamoto ^h, Ken Nakata ^h, Seiji Okada ^a, Kosuke Ebina ^{a,c,*}

^a Department of Orthopaedic Surgery, Osaka University Graduate School of Medicine, 2-2 Yamadaoka, Suita, Osaka 565-0871, Japan

^b Department of Gene & Stem Cell Regenerative Therapy, Osaka University Graduate School of Medicine, 2-2 Yamadaoka, Suita, Osaka 565-0871, Japan

^c Department of Sports Medical Biomechanics, Osaka University Graduate School of Medicine, 2-2 Yamadaoka, Suita, Osaka 565-0871, Japan

^d Department of Musculoskeletal Regenerative Medicine, Osaka University Graduate School of Medicine, 2-2 Yamadaoka, Suita, Osaka 565-0871, Japan

^e Department of Orthopaedic Surgery, Osaka Rosai Hospital, 1179-3 Nagasonecho, Kita-ku, Sakai, Osaka 591-8025, Japan

^f Clinical and Research Institute for Foot and Ankle Surgery, Jujo Hospital, 341-1 Mangoku, Kisarazu, Chiba 292-0003, Japan

^g Department of Orthopaedic Surgery, National Hospital Organization Osaka Minami Medical Center, 2-1 Kidohigashi-machi, Kawachinagano, Osaka 586-8521, Japan

^h Department of Medicine for Sports and Performing Arts, Osaka University Graduate School of Medicine, 2-2 Yamadaoka, Suita, Osaka 565-0871, Japan

ARTICLE INFO

Keywords:

RANKL
Postmenopausal osteoporosis
Osteoclast
Osteoblast
Osteocyte
Microglial healing peptide 1 with N-terminal acetylation and C-terminal amidation (MHP1-AcN)

ABSTRACT

Purpose: Estrogen deficiency following menopause increases receptor activator of nuclear factor-kappa B ligand (RANKL) expression in osteoblasts, thereby promoting osteoclast differentiation, and enhances T cell-derived tumor necrosis factor-alpha (TNF α) production, which induces sclerostin expression in osteocytes, thereby inhibiting bone formation. This study aimed to develop a novel uncoupling therapeutic agent for osteoporosis. **Methods:** We developed microglial healing peptide 1 with N-terminal acetylation and C-terminal amidation (MHP1-AcN), a modified RANKL peptide with N-terminal acetylation and C-terminal amidation lacking the osteoclast activating CD loop. Given the structural similarities of RANK and TNF receptor 1 (TNFR1), we hypothesized that MHP1-AcN could inhibit both the RANKL-RANK and TNF α -TNFR1 pathways to address the pathophysiology of osteoporosis, as evaluated in vitro and in vivo using an ovariectomized mouse model. **Results:** In ovariectomized mice, MHP1-AcN inhibited osteoclastogenesis, reduced osteocytic sclerostin expression, prevented bone loss, and improved the femoral cancellous and cortical bone microarchitecture. Unlike anti-RANKL antibody, MHP1-AcN considerably preserved bone formation by osteoblasts and enhanced bone strength, as evidenced by increases in energy absorption capacity. In vitro, MHP1-AcN bound to both RANK and TNFR1, suppressing osteoclast activity via the RANKL-RANK pathway and reducing sclerostin expression through the TNF α -TNFR1-nuclear factor-kappa B pathway. MHP1-AcN did not affect osteoblast proliferation and differentiation or RANKL expression. **Conclusion:** MHP1-AcN effectively inhibits osteoclastogenesis and sclerostin-mediated suppression of bone formation while considerably preserving osteoblast function. These findings suggest that MHP1-AcN, which targets dual pathways critical for bone homeostasis, is a promising uncoupling therapeutic agent for osteoporosis.

1. Introduction

Estrogen deficiency following menopause increases receptor activator of nuclear factor-kappa B ligand (RANKL) expression in osteoblasts [1]. RANKL binds to receptor activator of nuclear factor-kappa B

(RANK) on osteoclasts, activating nuclear factor-kappa B (NF- κ B) and MAPK signaling pathways via TRAF6, thereby promoting osteoclast differentiation and activation [2]. Concurrently, estrogen deficiency enhances tumor necrosis factor-alpha (TNF α) production by T cells [3]. TNF α binds to TNF receptor 1 (TNFR1) on osteocytes, inducing

* Corresponding author at: Department of Orthopaedic Surgery, Osaka University Graduate School of Medicine, 2-2 Yamadaoka, Suita, Osaka 565-0871, Japan.
E-mail address: k-ebina@ort.med.osaka-u.ac.jp (K. Ebina).

<https://doi.org/10.1016/j.bone.2025.117440>

Received 30 December 2024; Received in revised form 25 February 2025; Accepted 26 February 2025

Available online 1 March 2025

8756-3282/© 2025 The Authors. Published by Elsevier Inc. This is an open access article under the CC BY-NC-ND license (<http://creativecommons.org/licenses/by-nc-nd/4.0/>).

sclerostin expression through NF- κ B signaling, which inhibits Wnt signaling and suppresses bone formation [4].

Bisphosphonates and the anti-RANKL antibody denosumab both inhibit osteoclast activity and suppress osteoblast-driven bone formation through coupling inhibition [5]. Their prolonged use is sometimes associated with severe adverse events, such as osteonecrosis of the jaw and atypical femoral fractures [6,7]. Bone anabolic agents such as teriparatide stimulate bone formation; however, they also enhance RANKL production by osteoblasts, thereby increasing osteoclast activity and cortical porosity [8,9]. The anti-sclerostin antibody romosozumab promotes bone formation and suppresses resorption through an uncoupling effect via the Wnt signaling, but it also carries risks of cardiovascular events [10], highlighting the need for novel therapeutic strategies.

We and others demonstrated that RANKL inhibited Toll-like receptor (TLR) signaling to exert anti-inflammatory effects [11–13]. To repurpose RANKL for anti-inflammatory therapy, we developed microglial healing peptide 1 with N-terminal acetylation and C-terminal amidation (MHP1-AcN) by removing the CD loop, the osteoclast activation site, from murine RANKL [14]. MHP1-AcN exerts anti-inflammatory effects similar to RANKL, by inhibiting TLR4-induced inflammation by binding to CD14, which competes with LPS for CD14 binding. As a result, MHP1-AcN has displayed therapeutic efficacy in disease models, including ischemic stroke [14], psoriasis [15], and sepsis-induced acute lung injury [16].

In this study, we focused on the structural homology in the ligand-binding domains of RANK and TNFR1, as RANKL belongs to the TNF α superfamily [17]. We hypothesized that MHP1-AcN could ameliorate osteoporosis pathology by competitively inhibiting the RANKL–RANK pathway to suppress osteoclast differentiation and the TNF α –TNFR1 pathway to reduce sclerostin expression in osteocytes. This study aimed to elucidate the therapeutic effects and underlying mechanisms of MHP1-AcN in a postmenopausal osteoporosis mouse model.

2. Methods

2.1. Peptide design and synthesis

MHP1-AcN (Ac-LMVYVVKTSIKIPSSHNLMKGGSTKNWGSN-NH₂) was obtained from ILS (Ibaraki, Tsukuba, Japan). The peptide was dissolved in double-distilled water at a concentration of 4 mg/ml and stored at 4 °C. Prior to experimental use, the solution was diluted 1:1 with physiological saline [14,16].

2.2. Experimental design and the animal model

Seven-week-old female C57BL/6J mice were obtained from Charles River Laboratories (Wilmington, MA, USA). After a 1-week acclimatization period, the mice were subjected to sham surgery or ovariectomy (OVX). Anesthesia and surgical procedures were performed following established protocols [18,19].

The mice were randomly divided into five groups ($n = 7$ – 8 /group): sham + saline [subcutaneous (s.c.) PBS and intraperitoneal (i.p.) saline], sham + MHP1-AcN (s.c. PBS and i.p. MHP1-AcN), OVX + saline (s.c. PBS and i.p. saline), OVX + MHP1-AcN (s.c. PBS and i.p. MHP1-AcN), and OVX + murine RANKL monoclonal antibody (anti-RANKL ab; i.p. anti-RANKL ab and i.p. saline). Treatments were administered for 4 weeks post-surgery starting for the day after surgery (Day1) as a volume of 200 μ l of PBS or anti-RANKL ab (300 μ g/kg, Oriental Yeast Co., Tokyo, Japan) given subcutaneously 2 times/week and 300 μ l of saline or MHP1-AcN (30 mg/kg) given intraperitoneally 5 times/week. The doses of anti-RANKL ab and MHP1-AcN were based on previous studies [16,20]. The mice were sacrificed at 4 weeks post-surgery for evaluation.

2.3. Immunofluorescence staining of knee joint tissues

Mice were randomly divided into the control (300 μ l of i.p. saline) and FITC-MHP1-AcN groups (300 μ l of i.p. FITC-MHP1-AcN solution). Fifteen minutes after injection, the mice were euthanized, and tissues were collected for further processing. Frozen sagittal sections of mouse knee joints were prepared using the Kawamoto method [21].

Immunofluorescence staining was performed using the biotin–avidin amplification technique. Detailed information on tissue section washing, blocking, antibody treatments, and image acquisition procedures is presented in the supplementary material.

2.4. Microcomputed tomography (μ CT)

The distal femurs of mice were analyzed using a high-resolution μ CT scanner (SkyScan 1272; Bruker, Kontich, Belgium). μ CT was performed using the following consistent parameters: a scan resolution of 10 μ m per voxel, μ CT settings of 90 kV and 160 mA. The scan speed was set with a rotation step of 0.6° (180° rotation), and the acquisition time per sample was approximately 5 min.

The region of interest (ROI) was defined as starting 500 μ m from the growth plate, extending proximally for a total of 1000 μ m. Trabecular parameters, including the bone volume (BV)/tissue volume (TV) ratio (%), trabecular number (Tb. N, N/mm), trabecular separation (Tb. Sp, mm), and trabecular thickness (Tb. Th, mm) were evaluated using SkyScan CT Analyzer software (Billerica, MA, USA), as previously described [22].

2.5. Histological and immunohistochemical analyses

The protocol for the quantitative assay was conducted as previously described [23]. Following μ CT, the femurs were fixed in formalin, decalcified, and embedded. Tartrate-resistant acid phosphatase (TRAP) staining (Cosmo Bio, Tokyo, Japan) was performed according to the manufacturer's protocol. Immunostaining was conducted using primary antibodies against osteocalcin, sclerostin, and TNF α following the manufacturers' protocols. Sections were then incubated with a secondary antibody (VECTASTAIN ABC Rabbit IgG Kit, PK-4005, Vector Laboratories, Newark, CA, USA) and stained with 3,3'-diaminobenzidine tetrahydrochloride (Nichirei Bioscience, Tokyo, Japan). The antibodies used in this study are listed in Supplementary Table 1.

The same region analyzed by μ CT was examined histologically. Within this region, TRAP-positive cells and osteocalcin-positive cells were counted on five randomly selected trabecular bone surfaces, whereas the percentages of sclerostin-positive and TNF α -positive osteocytes were evaluated for all osteocytes in the cortical bone as described in previous studies [18,22].

2.6. Histomorphometrical analysis

To label active bone formation, all mice were subcutaneously injected with tetracycline (20 mg/kg) and calcein (10 mg/kg), respectively, 5 days and 2 days before sacrifice, as described in a previous study [24].

The femurs were extracted, fixed in 70 % ethanol, treated with Villanueva bone stain, and embedded in methacrylate (Wako Pure Chemical Industries, Osaka, Japan).

The following histomorphometric parameters were measured as previously described [23]: number of osteoclasts (Oc. N, N/mm), number of multinucleated osteoclasts (M.Oc. N, N/mm), eroded surface (ES)/bone surface (BS) ratio (%), number of osteoblasts (Ob. N) (N/mm), osteoid thickness (O.Th, μ m), mineralizing surface (MS)/bone surface (BS) ratio (%), bone formation rate (BFR)/bone surface (BS) ratio ($\text{mm}^3/\text{mm}^2/\text{year}$), and mineral apposition rate (MAR, $\mu\text{m}/\text{day}$).

The standard bone histomorphometric nomenclature, symbols, and units were used as described previously [25].

2.7. Three-point bending test

The femoral mechanical properties were assessed using a three-point bending test (ElectroForce 5500; TA Instruments, New Castle, DE, USA). The bone samples were frozen upon collection and thawed before conducting the three-point bending test. Bones were positioned on two fixed loading points 8 mm apart, with the upper loading point centered between them.

A constant displacement rate of 0.1 mm/s was applied until fracture. Load displacement data were recorded to calculate the maximum load (N), stiffness (N/mm), energy absorption (N·mm), and fracture displacement (mm), as described previously [26].

2.8. Reagents and cell culture

Mouse bone marrow mononuclear cells (BMMCs) were isolated from the femurs and tibiae of 8-week-old female C57BL/6J mice as previously described [18]. The cells were cultured in α -minimum essential medium (α -MEM, Nacalai Tesque, Kyoto, Japan) containing 10 % fetal bovine serum (FBS, Equitech-Bio, Kerrville, TX, USA) and 1 % antibiotic/antimycotic solution (A/A, Sigma-Aldrich, St. Louis, MO, USA) with 5 ng/ml macrophage colony-stimulating factor (M-CSF, R&D Systems, Minneapolis, MN, USA).

NF- κ B luciferase-stable RAW 264.7 cells were obtained from AnGes (Ibaraki, Japan) and maintained in RPMI 1640 medium (Thermo Fisher Scientific, Waltham, MA, USA) containing 10 % FBS and 100 ng/ml hygromycin B (Nacalai Tesque).

MC3T3-E1 osteoblastic cells were obtained from the Riken Cell Bank (RIKEN BioResource Research Center, Tsukuba, Ibaraki, Japan) and maintained in α -MEM containing 10 % FBS and 1 % A/A.

Saos-2 osteosarcoma cells were obtained from the Riken Cell Bank and maintained in Dulbecco's modified Eagle's medium (Nacalai Tesque) containing 10 % FBS and 1 % A/A.

All cells were cultured at 37 °C in a humidified atmosphere with 5 % carbon dioxide. For all cell types, MHP1-AcN was added 2 h prior to stimulation with other reagents. Approximately, the plasma concentration of MHP1-AcN was reported to reach approximately 8 μ g/ml 30 min after intravenous injection at a dose of 2 mg/ml (10 ml/kg) in mice [14]. Our chosen *in vitro* concentrations of MHP1-AcN encompassed this physiologically relevant range, and they were consistent with those used in previous *in vitro* reports [16,27,28].

2.9. *In vitro* osteoclast differentiation and TRAP staining

BMMCs were seeded in 24-well plates at a density of 1×10^5 cells/well and stimulated with 10 ng/ml M-CSF and 50 ng/ml RANKL (R&D Systems) to induce osteoclastogenesis, with or without MHP1-AcN (10, 30, or 100 μ g/ml), for 5 days.

TRAP staining was performed using a TRAP staining kit (Cosmo Bio, Tokyo, Japan) according to the manufacturer's protocol. The total number of TRAP-positive cells with three or more nuclei was determined as described previously [18].

2.10. RNA sequencing

RNA sequencing was performed as previously described [22]. Sequencing was conducted on the Illumina NovaSeq 6000 platform (Illumina, San Diego, CA, USA). Reads were aligned to the hg19 genome, and differential expression analysis was performed. Further details on RNA extraction, library preparation, sequencing parameters, and data analysis are provided in the supplementary material.

2.11. Western blotting

The protocol for western blotting followed the methodology outlined in a previous publication [29]. Cytoplasmic and nuclear extracts were

prepared using the NE-PER kit (Pierce, Rockford, IL, USA) according to the manufacturer's protocol. The primary antibodies used in this study are listed in Supplementary Table 1.

2.12. Quantitative real-time polymerase chain reaction (RT-qPCR) assay

The RT-qPCR protocol was described in a previous study [22]. The primer sequences are provided in Supplementary Table 2, and further details are presented in the supplementary material.

2.13. Luciferase assay

2.13.1. Luciferase assay in NF- κ B luciferase-stable RAW 264.7 cells

NF- κ B luciferase-stable RAW 264.7 cells were seeded in 96-well plates at a density of 1×10^4 cells/well. The cells were stimulated with 50 ng/ml RANKL, with or without MHP1-AcN (10, 30, or 100 μ g/ml), for 6 h. Then, Steady-Glo reagent (Promega, Madison, WI, USA) was added to each well, and luminescence was measured using a Centro XS3 LB960 luminometer (Berthold Technologies GmbH & Co. KG, Bad Wildbad, Germany) after a 5-min incubation period as described previously [16,23].

2.13.2. Luciferase assay in MC3T3-E1 and Saos-2 cells for transient transfection

The luciferase assay was performed as describe previously [22]. MC3T3-E1 and Saos-2 cells were transiently transfected with the κ B-Luc2P plasmid (pGL4.15; Promega) via electroporation. Cells were incubated with or without MHP1-AcN, followed by stimulation with or without TNF α (10 ng/ml, R&D Systems). Luminescence was measured using a Centro XS3 LB960 luminometer after adding Steady-Glo reagent. Further details on cell preparation, electroporation parameters, incubation times, and measurement procedures are provided in the supplementary material.

2.14. Alkaline phosphatase (ALP) staining, ALP activity, and cell proliferation assay

MC3T3-E1 cells were seeded in 24-well plates at a density of 1×10^5 cells/well and stimulated with 10 mM β -glycerophosphate (Calbiochem, San Diego, CA, USA) and 50 μ g/ml ascorbic acid (Sigma, St. Louis, MO), with or without MHP1-AcN (3, 10, or 30 μ g/ml), for 3 days.

After fixation in 10 % formalin, the cells were washed twice with PBS, and ALP staining was performed using BCIP/NBT Color Development Substrate (Promega).

In parallel experiments, ALP activity was measured using the BCA Protein Assay Kit (Thermo Fisher Scientific), and cell proliferation was assessed using Count Reagent SF (Nacalai Tesque), following the manufacturers' protocols.

2.15. Assessment of the effects of MHP1-AcN on RANKL expression

To examine the effects of MHP1-AcN on RANKL expression, MC3T3-E1 cells were stimulated with TNF α (10 ng/ml), with or without MHP1-AcN (3, 10, or 30 μ g/ml), for 24 h. In parallel experiments, western blotting was conducted to assess phosphorylated p65, total p65, phosphorylated I κ B α , and total I κ B α expression after 1 h of stimulation with TNF α (1 ng/ml).

2.16. Assessment of sclerostin expression in stimulated Saos-2 cells

Saos-2 cells were seeded in six-well plates at a density of 1.0×10^6 cells/well and in 24-well plates at a density of 1.0×10^5 cells/well. To induce osteocytogenesis and sclerostin expression, the cells were cultured in medium containing 5 mM β -glycerophosphate and 50 μ g/ml ascorbic acid. Cells were then treated with or without TNF α (1 or 10 ng/ml) to stimulate sclerostin expression and in the presence or absence of

MHP1-AcN (3, 10, or 30 $\mu\text{g/ml}$) to evaluate its effects on $\text{TNF}\alpha$ -induced sclerostin expression. The experimental setup was based on a previously described method [22]. These experiments were conducted to specifically evaluate the response of Saos-2 cells to $\text{TNF}\alpha$ stimulation by

culturing them alone.

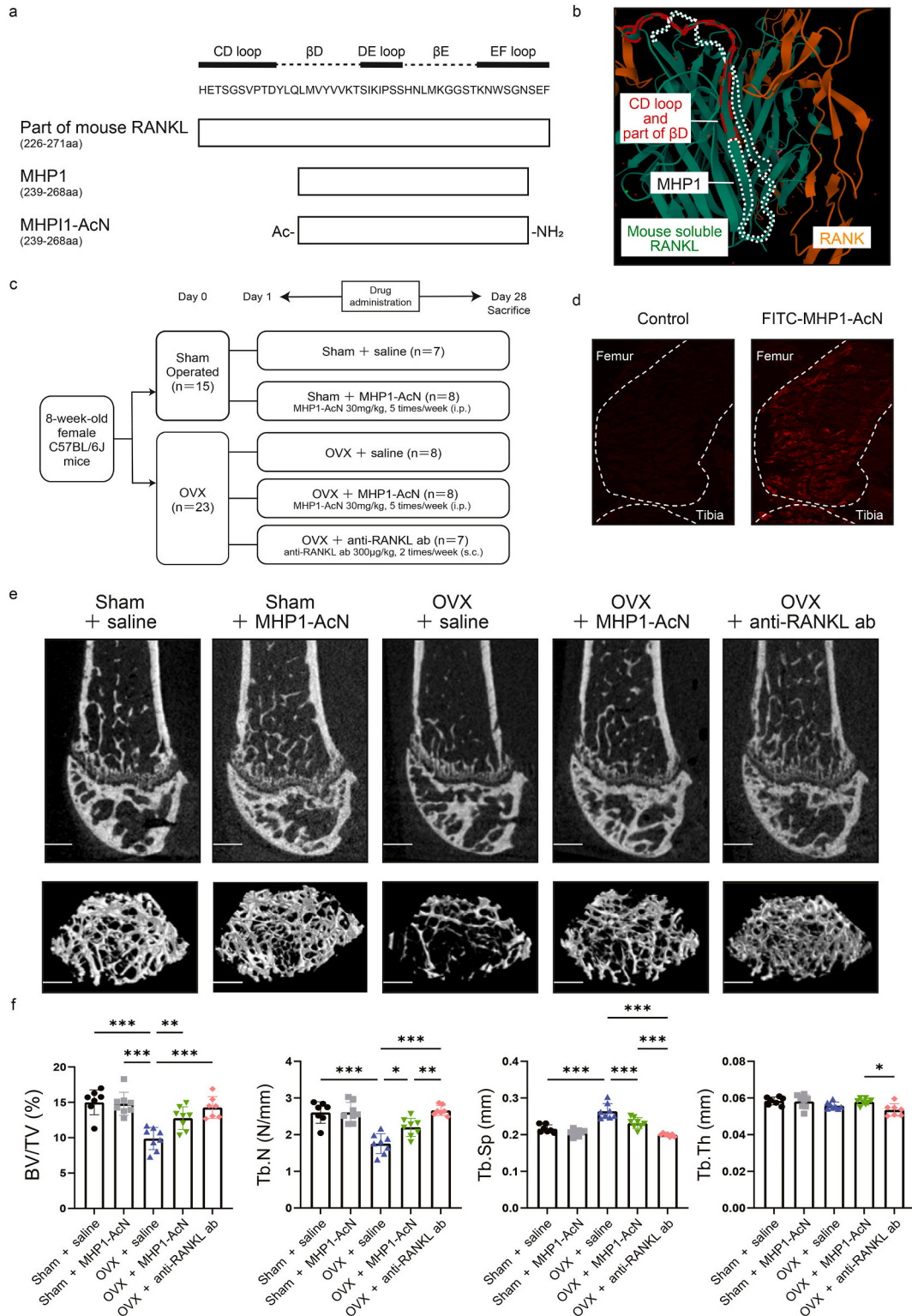


Fig. 1. Effects of MHP1-AcN on OVX mice.

(a) Schematic representations of part of mouse RANKL, microglial healing peptide 1 (MHP1), and MHP1-AcN. (b) Three-dimensional structures of the CD loop and part of βD , MHP1, mouse soluble RANKL, and RANK. (c) Experimental protocol. (d) Immunofluorescence staining of FITC-labeled MHP1-AcN in the knee joint. (e) Representative μCT images of the distal femur in the five groups after the intervention. Scale bar: 500 μm . (f) Quantification of trabecular bone parameters: BV/TV (%), Tb. N (N/mm), Tb. Sp (mm), and Tb. Th (mm). Data are expressed as the mean \pm SD ($n = 7$ or 8).

2.17. Immunofluorescence staining of Saos-2 cells

Saos-2 cells were seeded in 24-well plates at a density of 5.0×10^3 cells/well. After 24 h of incubation, the cells were treated with/without TNF α and MHP1-AcN. After 0.5 h of treatment, immunofluorescence staining was performed as described previously [22]. Cell images were acquired using an IN Cell Analyzer 6000 (GE Healthcare, Chicago, IL, USA), capturing 16 view fields per well. The Nuc/Cyto ratio of the NF- κ B signal was calculated using the mean signal intensity of the nuclear and cytoplasmic areas in cells in each field per well.

2.18. Immobilization of TNFR1 on the sensor surface and binding of MHP1-AcN to TNFR1

Surface plasmon resonance (SPR) analysis was conducted using a Biacore T200 system (GE Healthcare). Recombinant human TNFR1 was immobilized on a CM5 sensor chip. The binding of MHP1-AcN to TNFR1 was measured using single-cycle kinetics with MHP1-AcN concentrations of 0–65.2 μ g/ml. Data were analyzed using Biacore T200 Evaluation Software. Detailed information on TNFR1 immobilization, buffer compositions, injection parameters, and data analysis procedures is presented in the supplementary material.

2.19. Statistical analysis

The data are presented as the mean \pm SD. To compare the parameters across the groups, one-way analysis of variance with the Tukey–Kramer post hoc test and Mann–Whitney *U* test were employed. All statistical analyses were conducted using GraphPad Prism 9 (GraphPad, San Diego, CA, USA), with significance defined as $P < 0.05$.

The statistical power ($1-\beta$) was set at 80 %, and the significance level was set as 0.05 for all experiments. Sample sizes for each experiment were determined by power analysis, and the adequacy of these sample sizes was supported by post-hoc power analysis of the actual data (effect size >0.8 , actual power > 80 %).

2.20. Study approval

All experimental protocols comply with the ARRIVE guidelines and were approved by the Animal Experimental Committee of Osaka University (number: 02-057-013, date: August 27, 2020).

3. Results

3.1. Structure of MHP1-AcN

We developed MHP1-AcN, a modified partial peptide of mouse RANKL designed to inhibit TLR4-induced inflammation without activating osteoclasts [14]. The peptide does not contain RANKL's CD loop (responsible for osteoclastogenesis [30]), but it includes the DE loop and part of the EF loop (crucial for RANK binding [30], Fig. 1a). MHP1-AcN features an N-terminal acetyl group and a leucine-to-valine substitution for enhanced stability and anti-inflammatory effects [14] without promoting osteoclastogenesis [27]. The 3D structural model was constructed using Protein Data Bank Europe data (Fig. 1b).

3.2. Effects of MHP1-AcN on OVX mice

The mice were randomly assigned to five groups, as presented in Fig. 1c. To assess the effects of MHP1-AcN administration in OVX mice, we first evaluated its impact on body weight, finding no significant differences between and after MHP1-AcN treatment (Supplementary Fig. 1a).

FITC-labeled MHP1-AcN was administered intraperitoneally, and the knee joint was harvested. Immunofluorescent staining of frozen sections revealed that MHP1-AcN migrated to the bone marrow (Fig. 1d).

μ CT of the distal femur on day 28 (Fig. 1e and f) revealed that the OVX + saline group had significantly lower BV/TV and Tb. N and higher Tb. Sp than the sham + saline group. These parameters were significantly improved in the OVX + MHP1-AcN group compared with those in the OVX + saline group. The OVX + anti-RANKL ab group exhibited greater improvements in Tb. N and Tb. Sp, although the improvement in BV/TV was not statistically significant, whereas Tb. Th was lower in this group than in the OVX + MHP1-AcN group. Additionally, in the sham group, administration of MHP1-AcN did not exhibit significant effects on trabecular parameters measured compared to those in the saline group.

TRAP staining of osteoclasts in the trabecular bone of the distal femur revealed a significantly higher number of TRAP-positive multinucleated cells in the OVX + saline group than in the sham + saline group. OVX + MHP1-AcN reduced the number of TRAP-positive cells, whereas OVX + anti-RANKL ab further decreased the number of these cells (Fig. 2a).

Histomorphometric analysis of the distal femur (Fig. 2b and Supplementary Fig. 1b–e) demonstrated that large numbers of osteoclasts surrounded the bone fragments in the OVX + saline group. The OVX + saline group featured significantly higher Oc. N, M.Oc. N, and ES/BS than the sham + saline group, whereas OVX + MHP1-AcN reduced all of these parameters (Fig. 2b and c).

In the distal femur trabecular bone, osteocalcin immunostaining revealed a significantly higher number of osteocalcin-positive cells in the OVX + saline group than in the sham + saline group. Of note, OVX + MHP1-AcN slightly increased the number of osteocalcin-positive cells compared with that in the OVX + saline group, while OVX + anti-RANKL ab markedly suppressed their counts (Fig. 2d).

The number of osteoblasts was higher in the OVX + saline group than in the sham + saline group, and the number of osteoblasts was further elevated in the OVX + MHP1-AcN group. Both MAR and BFR/BS were higher in the OVX + saline group than in the sham + saline group. These values remained significantly higher relative to those in the sham + saline group, although they were slightly suppressed in the OVX + MHP1-AcN group (Fig. 2e and f). Similar trends were observed for other bone formation parameters (Supplementary Fig. 1f).

Sclerostin-positive cell counts in cortical bone were significantly higher in the OVX + saline group than in the sham + saline group. OVX + MHP1-AcN significantly reduced the number of sclerostin-positive cells, although the number of sclerostin-positive cells was similar in the OVX + anti-RANKL ab and OVX + saline groups (Fig. 2g). By contrast, immunohistochemistry revealed no significant difference in the number of TNF α -positive osteocytes between the OVX + saline and OVX + MHP1-AcN groups (Supplementary Fig. 1g), indicating that MHP1-AcN did not affect TNF α expression.

Fig. 2h presents the results of the three-point bending test for various femoral biomechanical properties. Energy absorption and fracture displacement were lower in the OVX + saline and OVX + anti-RANKL ab groups than in the sham + saline group, although OVX + MHP1-AcN prevented the declines in these parameters. These findings suggest that MHP1-AcN, but not anti-RANKL ab, reversed the reductions in femur biomechanical properties induced by OVX. Conversely, maximum load and stiffness did not differ among the groups (Supplementary Fig. 1h). To further investigate the effects of MHP1-AcN on cortical bone, we conducted a detailed histomorphometric analysis in a more proximal region, closer to the site likely contributing to the three-point bending test (Supplementary Fig. 2). This analysis revealed that MHP1-AcN significantly increased cortical width (Supplementary Fig. 2a and b) and maintained the mineral apposition rate on cortical bone surfaces (Supplementary Fig. 2c and d), while also reduced the porosity of the cortical area (Supplementary Fig. 2e). These findings align with the results of three-point bending test.

3.3. Effects of MHP1-AcN on osteoclasts

Fig. 3a illustrates the experimental designs used to evaluate the

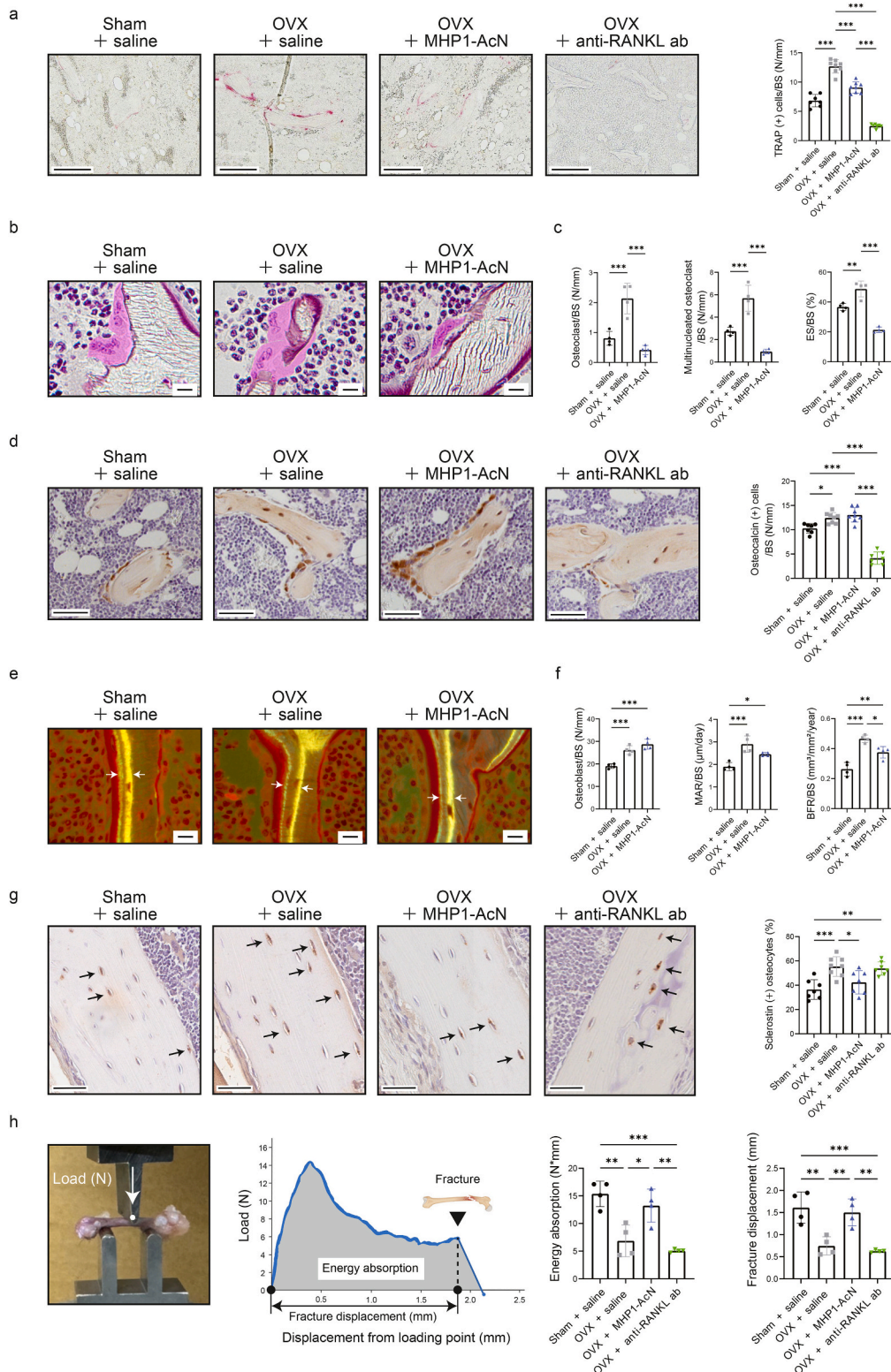


Fig. 2. Histological, histomorphometric, and immunohistochemical analyses of the distal femur were conducted in each group, and the femoral biomechanical structural properties were assessed using a three-point bending test.

(a) Histological, (b and e) histomorphometric, and (d and g) immunohistochemical analyses. (a) TRAP staining. Data are expressed as the mean \pm SD ($n = 7$ or 8). Scale bar: $100 \mu\text{m}$. (b) Villanueva bone staining. Osteoclasts and trabecular bone were stained pink via computer image processing. Scale bar: $10 \mu\text{m}$. (c) Trabecular bone parameters, including Oc. N (N/mm), M.Oc. N (N/mm), and ES/BS (%), were quantified. Data are expressed as the mean \pm SD ($n = 4$). (d) Osteocalcin staining. Data are expressed as the mean \pm SD ($n = 7$ or 8). Scale bar: $50 \mu\text{m}$. (e) Images of the MAR under fluorescent light (white arrows indicate double-labeled surface). Scale bar: $10 \mu\text{m}$. (f) Trabecular bone parameters, including Ob. N (N/mm), MAR ($\mu\text{m}/\text{day}$), and BFR/BS ($\text{mm}^3/\text{mm}^2/\text{year}$), were quantified. Data are expressed as the mean \pm SD ($n = 4$). (g) Sclerostin staining (black arrows indicate sclerostin-positive osteocytes). Data are expressed as the mean \pm SD ($n = 7$ or 8). Scale bar: $50 \mu\text{m}$. (h) The three-point bending test (white dot indicates loading point), including energy absorption ($\text{N}\cdot\text{mm}$) and fracture displacement (mm). Data are expressed as the mean \pm SD ($n = 4$). (For interpretation of the references to colour in this figure legend, the reader is referred to the web version of this article.)

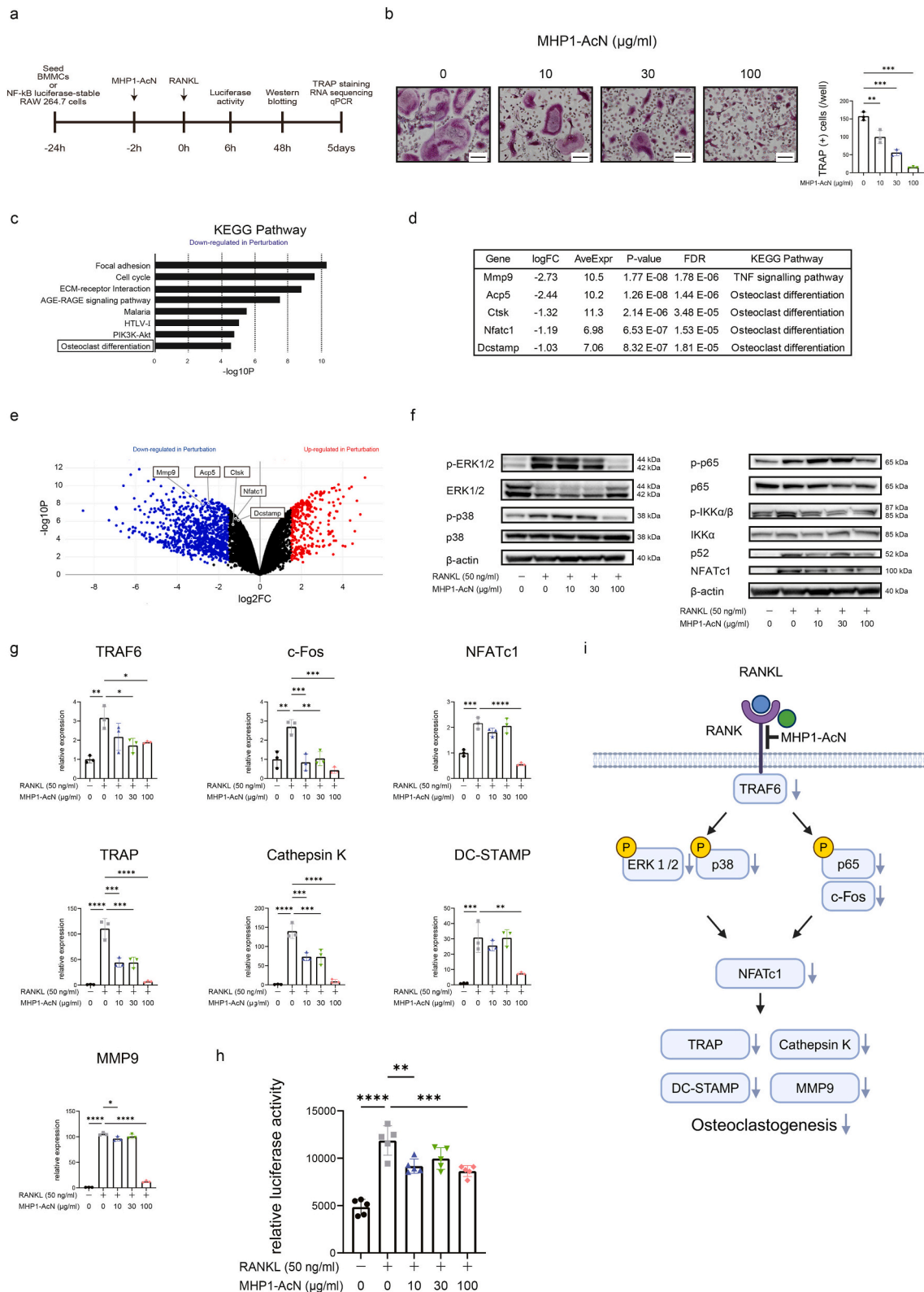


Fig. 3. Effects of MHP1-AcN on osteoclasts.

(a) Experimental protocol. (b) TRAP staining of mouse BMMCs cultured with M-CSF (10 ng/ml) and RANKL (50 ng/ml), with or without different concentrations of MHP1-AcN, for 5 days. Scale bar: 100 μm . (c) KEGG pathway analysis results of the eight most downregulated pathways identified from RNA sequencing data in the presence of MHP1-AcN (100 $\mu\text{g/ml}$) under RANKL (50 ng/ml) stimulation in BMMCs. (d) Potential of MHP1-AcN to regulate *Mmp9*, *Acp5*, *Ctsk*, *Nfatc1*, and *Dcstamp* as identified by RNA sequencing in BMMCs. (e) Volcano plot displaying the differentially expressed transcripts between RANKL and RANKL + MHP1-AcN groups. (f) Western blotting of BMMCs cultured with M-CSF (10 ng/ml) and RANKL (50 ng/ml), with or without different concentrations of MHP1-AcN, for 48 h. (g) Changes in the expression of genes involved in osteoclast differentiation were assessed. Data are expressed as the mean \pm SD ($n = 3$). (h) NF- κ B luciferase-stable RAW 264.7 cells were incubated with RANKL (50 ng/ml), with or without different concentrations of MHP1-AcN, for 6 h. Luciferase activity was then measured. Data are expressed as the mean \pm SD ($n = 5$). (i) Schematic representation of the signaling pathways involved in osteoclast differentiation following MHP1-AcN treatment.

effects of MHP1-AcN. Specifically, BMMCs were used for the osteoclast differentiation assay, and NF- κ B luciferase-stable RAW 264.7 cells were used for the luciferase assays. TRAP staining demonstrated that MHP1-AcN significantly reduced the number of RANKL-induced osteoclasts in a concentration-dependent manner (Fig. 3b).

To further explore the mechanisms underlying the effects of MHP1-AcN on osteoclasts, RNA sequencing was performed using BMMCs treated with RANKL and RANKL + MHP1-AcN. KEGG pathway analysis identified the eight most downregulated pathways in each group, including the osteoclast differentiation signaling pathway (Fig. 3c). Notably, the expression of key osteoclast-related genes, including matrix metalloproteinase 9 (Mmp9), acid phosphatase 5 (Acp5), cathepsin K (Ctsk), Nfatc1, and dendritic cell-specific transmembrane protein (Dcstamp), was found to be significantly suppressed by MHP1-AcN treatment (Fig. 3d and e).

Western blotting indicated that MHP1-AcN inhibited the phosphorylation of ERK1/2, p38, and p65 in BMMCs. In addition, MHP1-AcN suppressed the phosphorylation of IKK α / β and NF- κ B p52, leading to decreased NFATc1 protein expression (Fig. 3f).

Fig. 3g presents the results of RT-qPCR for osteoclast-related mRNAs following MHP1-AcN treatment. MHP1-AcN inhibited the expression of osteoclastogenesis signaling-related mRNAs such as TRAF6, c-Fos, and NFATc1. In addition, the osteoclast markers TRAP, Ctsk, DC-STAMP, and MMP9 were significantly suppressed.

To confirm the inhibitory effect of MHP1-AcN on NF- κ B transcriptional activity, luciferase assays were conducted using NF- κ B luciferase-stable RAW 264.7 cells. MHP1-AcN significantly reduced RANKL-induced NF- κ B transcriptional activity (Fig. 3h).

We previously reported that MHP1-AcN binds to RANK [16]. The current study indicated that binding between MHP1-AcN and RANK might inhibit downstream RANKL-RANK signaling, including TRAF6, ERK, p38, p65, c-Fos, and NFATc1, thereby suppressing osteoclastogenesis (Fig. 3i).

3.4. Effects of MHP1-AcN on osteoblasts

We next investigated whether MHP1-AcN influences osteoblast differentiation and proliferation or RANKL expression (Fig. 4a). The experimental protocols used to evaluate the effects of MHP1-AcN on TNF α -stimulated osteoblasts are outlined in Fig. 4b.

ALP staining, ALP activity assays, and WST proliferation assays revealed that MHP1-AcN does not directly alter osteoblast differentiation and proliferation (Fig. 4c–e).

In TNF α -stimulated MC3T3-E1 cells, RT-qPCR demonstrated that MHP1-AcN did not alter the expression of ALP, RANKL, osteoprotegerin (OPG), and cyclooxygenase-2 (COX-2) or the RANKL/OPG ratio (Fig. 4f). Furthermore, western blotting indicated that MHP1-AcN did not affect I κ B α degradation or p65 phosphorylation (Fig. 4g). Consistently, in luciferase reporter assays, TNF α -induced NF- κ B transcriptional activity was not modulated by MHP1-AcN (Fig. 4h).

These results collectively indicate that MHP1-AcN does not directly impact osteoblast function or NF- κ B signaling in TNF α -stimulated osteoblasts.

3.5. Effects of MHP1-AcN on osteocytes

Fig. 5a presents a schematic representation of sclerostin expression in osteocytes. Fig. 5b outlines the experimental design, in which Saos-2 cells were used to evaluate the effects of MHP1-AcN on osteocytes.

After stimulation with TNF α , RT-qPCR of Saos-2 cells revealed that MHP1-AcN inhibited the expression of TNF receptor-associated death domain protein (TRADD), receptor-interacting protein kinase 1 (RIPK1), transforming growth factor beta-activated kinase 1 (TAK1), and sclerostin (Fig. 5c).

Furthermore, western blotting illustrated that MHP1-AcN suppressed the phosphorylation of IKK α / β after 10 min of TNF α stimulation

and the phosphorylation of I κ B α after 30 min. This suppression subsequently led to a decrease in the nuclear protein levels of NF- κ B, specifically inhibiting the nuclear expression of p65 (Fig. 5d).

Immunofluorescence staining demonstrated that MHP1-AcN significantly inhibited TNF α -induced NF- κ B p65 nuclear translocation in osteocytes. TNF α treatment increased the percentage of NF- κ B-activated osteocytes, which was significantly reduced by MHP1-AcN, demonstrating its ability to suppress osteocyte activation (Fig. 5e).

To further evaluate the impact of MHP1-AcN on the NF- κ B pathway, we performed a luciferase reporter assay using Saos-2 cells. TNF α administration significantly increased NF- κ B transcriptional activity, whereas MHP1-AcN treatment significantly reversed this effect (Fig. 5f).

To validate our SPR assay, we first tested TNF α binding to TNFR1 as a positive control. Supplementary Fig. 3a presents the concentration-dependent binding of TNF α to TNFR1. Then, we confirmed the specificity of the binding between MHP1-AcN and TNFR1, resulting in a concentration-dependent interaction. The equilibrium dissociation constant for this interaction was 2.15×10^6 M (Fig. 5g).

Our competitive binding experiments revealed that MHP1-AcN binds to TNFR1 without inhibiting TNF α binding (Supplementary Fig. 3b). We propose that MHP1-AcN modulates TNF α -TNFR1 signaling by disrupting TRADD-mediated signal transduction, resulting in the suppression of the NF- κ B pathway and a subsequent reduction in sclerostin expression in osteocytes (Fig. 5h). Furthermore, our experiments illustrated MHP1-AcN also suppresses TNF α -induced inflammatory cytokine production in BMMCs, supporting that MHP1-AcN inhibited TNF α -TNFR1 signaling (Supplementary Fig. 3c).

4. Discussion

In this study, we demonstrated that MHP1-AcN, a novel peptide derived from a partial sequence of RANKL, effectively suppressed bone loss and improved bone microarchitecture and strength in an OVX mouse model. MHP1-AcN inhibited osteoclast formation and suppressed sclerostin expression in osteocytes without affecting osteoblasts. Notably, MHP1-AcN inhibited both the RANKL-RANK and TNF α -TNFR1 signaling pathways to exert distinct effects.

In postmenopausal osteoporosis, RANKL expression is upregulated in osteoblasts [1], and it activates RANKL-RANK signaling in osteoclasts, thereby promoting osteoclastogenesis [2]. Many RANKL-binding drugs have been reported as promising novel therapeutic candidates targeting this pathway for osteoporosis treatment [31–33]. However, it has been suggested that long-term systemic RANKL inhibition can potentially cause excessive immunosuppression attributable to impaired lymph node development and reduced T cell function [34]. Moreover, discontinuation of long-term administration of the anti-RANKL antibody denosumab resulted in a marked increase in bone resorption caused by a reduction in OPG expression, leading to rapid bone loss [35]. Furthermore, the rebound effect is amplified by accumulated osteoclast precursors during the treatment period, which rapidly differentiate into mature osteoclasts upon the restoration of RANKL signaling [36]. These findings underscore the unresolved challenges in osteoporosis therapies targeting RANKL.

Meanwhile, RANK is highly and selectively expressed in monocyte-osteoclast lineage cells [37], suggesting that therapeutic approaches targeting RANK could be promising for osteoporosis treatment. However, RANK undergoes significant conformational changes when it binds to RANKL to initiate signal transduction. This dynamic characteristic has made it technically challenging to develop drugs targeting RANK to inhibit its interaction with RANKL [38].

The AA', CD, DE, and EF loops of RANKL are critical binding sites for RANK interactions, with inhibition of the DE loop binding capacity significantly reducing osteoclast activity and RANKL's binding affinity for RANK [14]. MHP1-AcN contains the DE loop and part of the EF loop [14], and we previously reported that MHP1-AcN binds to RANK [16]. In this study, we demonstrated that MHP1-AcN suppresses downstream

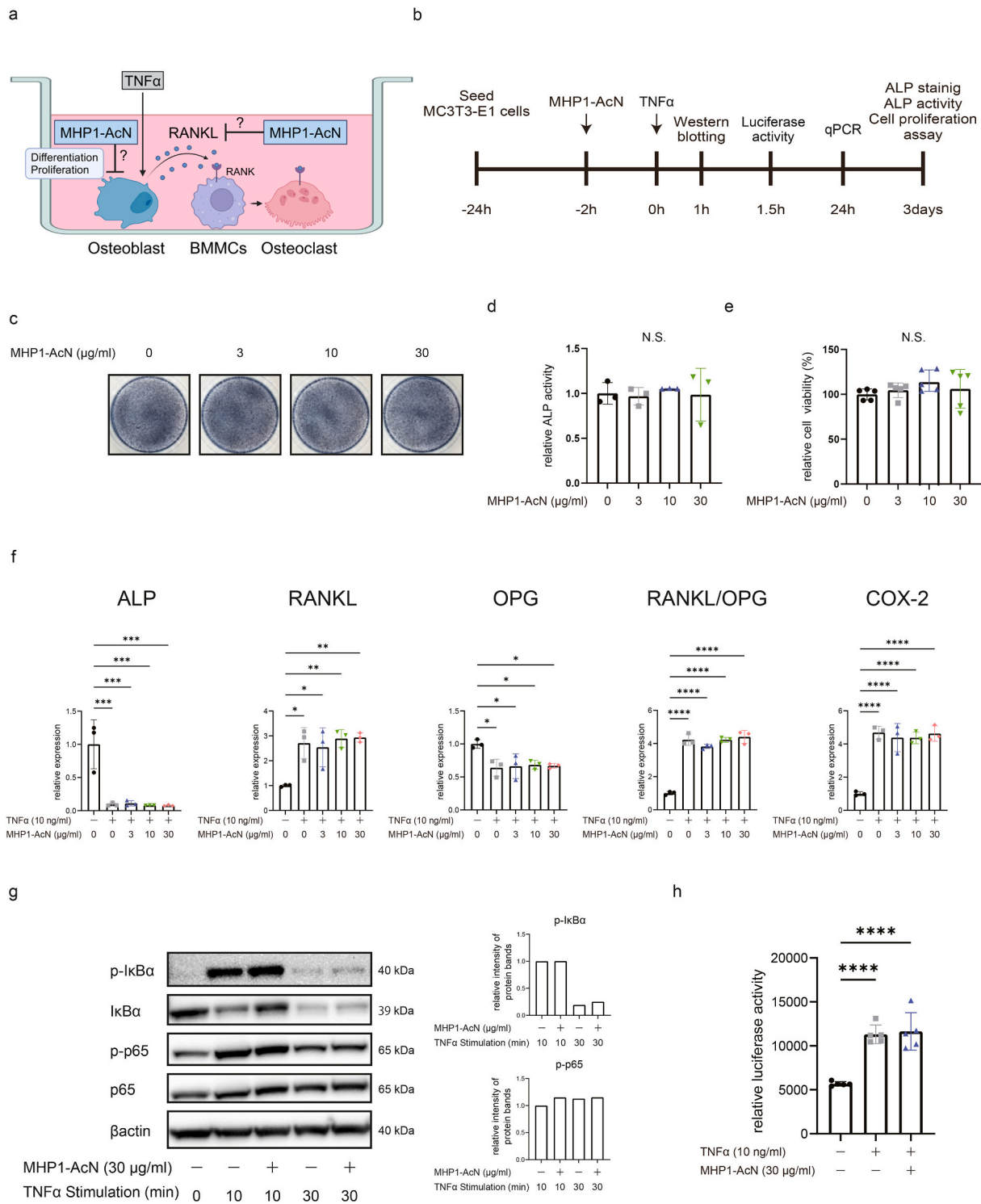


Fig. 4. Effects of MHP1-AcN on osteoblasts.

(a) Schematic representation of osteoclastogenesis induced by osteoblast-derived RANKL by TNF α and the inhibitory effect of MHP1-AcN. (b) Experimental protocol. (c) ALP staining of MC3T3-E1 cells cultured with 10 mM β -glycerophosphate and 50 μ g/ml ascorbic acid, with or without different concentrations of MHP1-AcN, for 3 days. (d) ALP activity assay in MC3T3-E1 cells incubated with or without different concentrations of MHP1-AcN for 3 days. Data are expressed as the mean \pm SD (n = 3). (e) Cell proliferation assay using MC3T3-E1 cells incubated with or without different concentrations of MHP1-AcN for 3 days. Data are expressed as the mean \pm SD (n = 5). (f) The mRNA expression of ALP, RANKL, OPG, and COX-2 and the RANKL/OPG ratio in MC3T3-E1 cells treated with TNF α (10 ng/ml), with or without different concentrations of MHP1-AcN, for 24 h. Data are expressed as the mean \pm SD (n = 3). (g) Western blotting of MC3T3-E1 cells cultured with TNF α (1 ng/ml), with or without different concentrations of MHP1-AcN, for 1 h. Volumetric analysis was performed utilizing β -actin as a loading control. (h) MC3T3-E1 cells were incubated with TNF α (10 ng/ml), with or without MHP1-AcN (30 μ g/ml), for 1.5 h. Luciferase activity was then measured. Data are expressed as the mean \pm SD (n = 5).

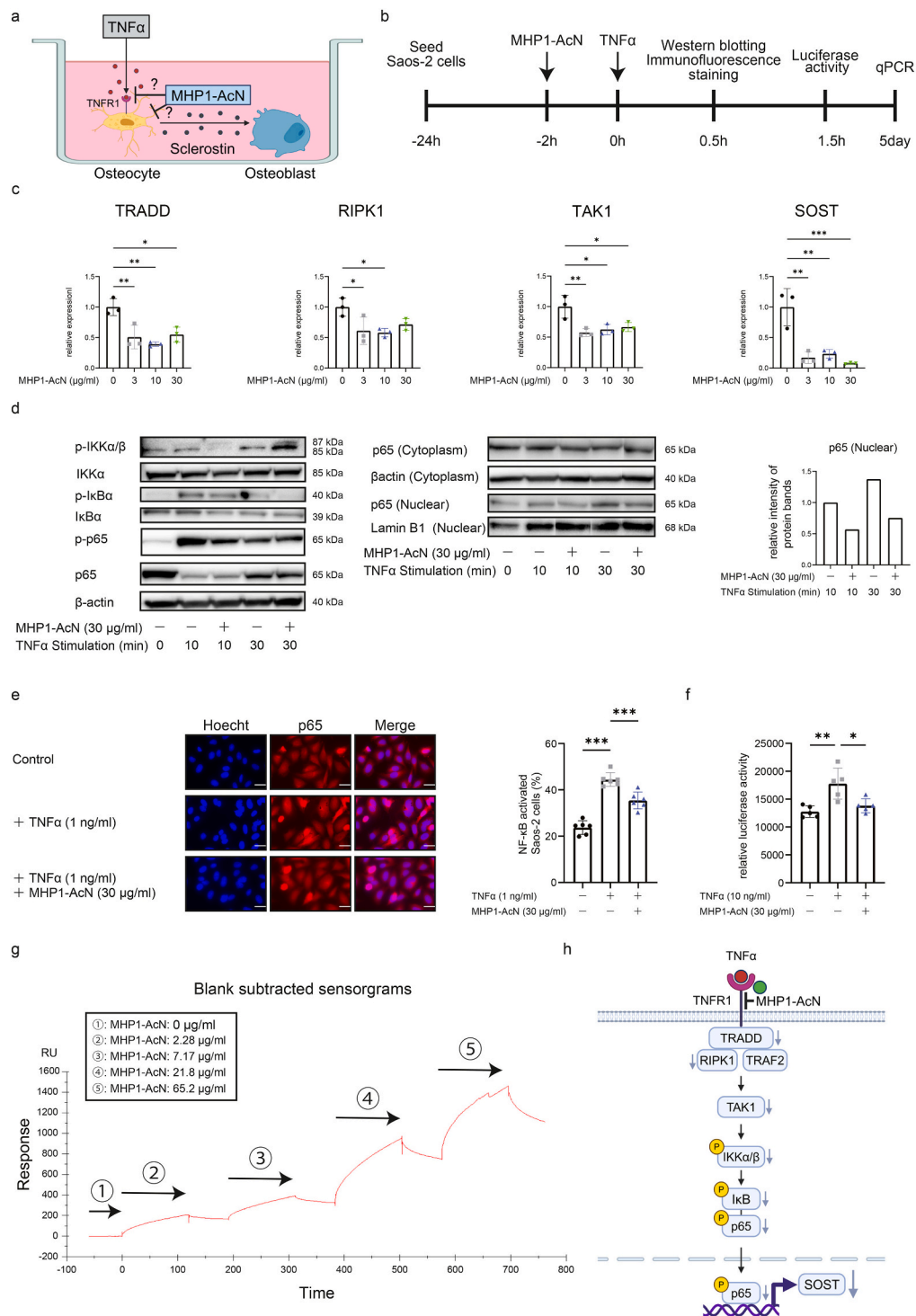


Fig. 5. Effects of MHP1-AcN on osteocytes. (a) Schematic representation of TNF α -induced sclerostin activity in osteocytes during estrogen deficiency and the inhibitory effect of MHP1-AcN treatment. (b) Experimental protocol. (c) mRNA expression of TRADD, RIPK1, TAK1, and sclerostin (SOST) in Saos-2 cells treated with TNF α (1 ng/ml), with or without different concentrations of MHP1-AcN, for 5 days. Data are expressed as the mean \pm SD ($n = 3$). (d) Western blotting of Saos-2 cells cultured with TNF α (1 ng/ml), with or without different concentrations of MHP1-AcN, for 10 or 30 min. Volumetric analysis was performed utilizing lamin B1 as a loading control. (e) Effects of MHP1-AcN on the nuclear translocation of NF- κ B p65 using immunofluorescence staining in Saos-2 cells cultured with TNF α (1 ng/ml), with or without MHP1-AcN (30 μ g/ml), for 30 min. Red, p65 immunofluorescent staining; blue, 4',6-diamidino-2-phenylindole (DAPI) nuclear staining. Scale bars: 30 μ m. The number of NF- κ B-activated Saos-2 cells relative to the total number of osteocytes imaged. Data are expressed as the mean \pm SD ($n = 6$). (f) Saos-2 cells were incubated with TNF α (10 ng/ml), with or without MHP1-AcN (30 μ g/ml), for 1.5 h. Luciferase activity was then measured. Data are expressed as the mean \pm SD ($n = 5$). (g) Target binding kinetics of MHP1-AcN. The binding affinity of MHP1-AcN for TNFR1 was assessed using SPR (Biacore T200). (h) Schematic representation of the signaling pathways leading to SOST expression in osteocytes following treatment with MHP1-AcN. (For interpretation of the references to colour in this figure legend, the reader is referred to the web version of this article.)

RANKL–RANK signaling by binding to RANK. Unlike existing RANKL-targeting therapies, direct regulation of RANK and its downstream functions by MHP1-AcN might offer several advantages: it could enable more selective inhibition of osteoclastogenesis and potentially minimize the systemic immunological effects associated with RANKL inhibition.

Following OVX, decreased estrogen levels result in increased TNF α production by T cells [3]. TNF α binds to TNFR1 on osteoblasts, activating NF- κ B, which subsequently binds to the COX-2 gene promoter, increasing COX-2 expression [39]. Elevated COX-2 levels enhance RANKL expression, promoting osteoclastogenesis [40]. In the present study, MHP1-AcN did not interfere with the TNF α –TNFR1–RANKL signaling pathway or the proliferation and differentiation of osteoblasts.

Conversely, TNF α –TNFR1 signaling in osteocytes leads to increased sclerostin expression and indirect inhibition of osteoblast-mediated bone formation [4]. RANK and TNFR1 belong to the TNFR superfamily and share structural similarities in their cysteine-rich domains (CRDs), which are crucial for ligand binding [17]. We hypothesized that these structural similarities between RANK and TNFR1 in their CRDs could explain MHP1-AcN's interaction with both receptors. Although developing small molecule drugs that competitively inhibit TNF α –TNFR1 binding has been challenging because of their high binding affinity [41], studies demonstrated that TNFR1 downstream signaling can be inhibited by modulating the receptor conformation without interfering with TNF α binding [42,43]. Our studies suggest that MHP1-AcN binds to TNFR1 in osteocytes and modulates its activity without blocking TNF α binding, thereby suppressing downstream signaling and reducing sclerostin expression. Based on our literature review, no previously reported therapeutic agents were documented to both bind to TNFR1 and exert anti-osteoporotic effects, underscoring the novelty of our findings.

Long-term suppression of bone remodeling can potentially compromise load-bearing capacity and bone strength [44]. Indeed, whereas denosumab suppresses bone remodeling, it has not been reported to improve femoral diaphyseal bone strength in ovariectomized cynomolgus monkeys [45]. In contrast to denosumab, MHP1-AcN improved energy absorption, a parameter of bone strength, as demonstrated in the three-point bending test. This effect is further supported by cortical bone analysis, which revealed increased width and reduced porosity.

The characteristics of MHP1-AcN, which inhibits excessive bone resorption while relatively maintaining bone formation through its anti-sclerostin effects, suggest that it can enhance bone strength more effectively than agents that inhibit RANKL through a single mechanism.

The effects of MHP1-AcN on OVX-induced osteoporosis are summarized in Fig. 6. MHP1-AcN inhibits osteoclastogenesis by blocking RANKL–RANK signaling and suppresses TNF α -induced sclerostin expression through TNF α –TNFR1 signaling, without directly affecting osteoblast function. This dual mechanism effectively reduces excessive bone resorption while relatively preserving bone formation, underscoring MHP1-AcN's potential as a novel uncoupling therapy for osteoporosis.

This study had several limitations. First, MHP1-AcN was administered only by i.p. injection based on previous studies [14–16]. Second, although we demonstrated short-term efficacy, long-term safety and efficacy remain unknown. Further studies in larger animals are needed to address these limitations before proceeding to human clinical trials. Third, MHP1-AcN was given preventively from Day 1 post-OVX, and its ability to restore lost bone mass remains unknown. Future studies should evaluate its therapeutic potential. Fourth, the impact of MHP1-AcN administration on serum OPG/RANKL balance and possibility for bone loss rebound after withdrawal remain unclear, which should be clarified in future studies. However, the strength of this study lies in its novel demonstration of MHP1-AcN's multitargeted approach against osteoporosis, providing a foundation for future therapeutic developments.

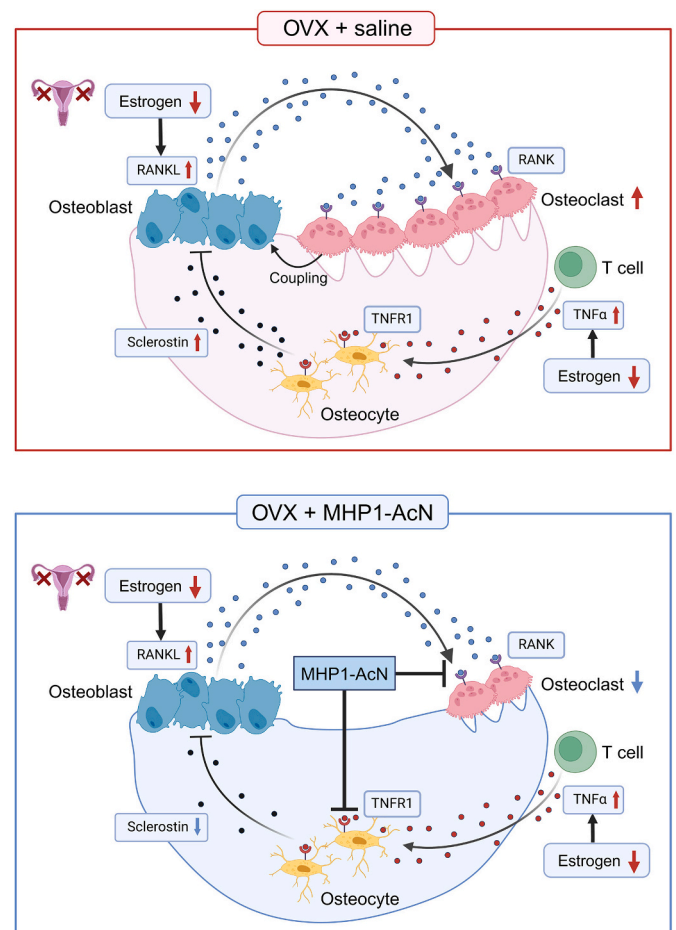


Fig. 6. Hypothesized scheme summarizing the effects of MHP1-AcN on osteoclasts, osteoblasts, and osteocytes in the context of OVX-induced osteoporosis.

5. Conclusion

Our findings suggest that MHP1-AcN, a novel peptide targeting both RANK and TNFR1, maintains balanced bone metabolism by suppressing excessive bone resorption while considerably preserving bone formation. This unique mechanism of action suggests that MHP1-AcN could represent a promising new therapeutic option for osteoporosis with potential clinical applications.

Supplementary data to this article can be found online at <https://doi.org/10.1016/j.bone.2025.117440>.

CRedit authorship contribution statement

Takuya Kurihara: Writing – original draft, Visualization, Validation, Resources, Methodology, Investigation, Formal analysis, Data curation, Conceptualization. **Munehisa Shimamura:** Supervision, Project administration, Methodology, Conceptualization. **Yuki Etani:** Supervision, Project administration, Methodology, Conceptualization. **Takaaki Noguchi:** Supervision, Project administration, Methodology, Conceptualization. **Yuji Fukuda:** Resources, Investigation. **Nagahiro Ochiai:** Resources, Investigation. **Atsushi Goshima:** Resources, Investigation. **Taihei Miura:** Resources, Investigation. **Makoto Hirao:** Supervision, Project administration, Methodology, Conceptualization. **Atsushi Sugimoto:** Resources, Investigation. **Nan Ju:** Supervision. **Satoshi Yamakawa:** Supervision. **Takashi Kanamoto:** Supervision. **Ken Nakata:** Supervision. **Seiji Okada:** Supervision. **Kosuke Ebina:** Writing – review & editing, Visualization, Project administration, Methodology, Conceptualization.

Funding

This work was funded by the Health and Labor Sciences Research Grant of Japan (grant number: 23K08651), Asahi Kasei Co., Ltd. and Eisai Co., Ltd. The Department of Gene & Stem Cell Regenerative Therapy is an endowed department supported by AS medical support. These funders played no roles in the study design, data collection and analysis, decision to publish, or preparation of the manuscript.

Declaration of competing interest

KE has received research grants from Asahi Kasei Co., Ltd., Eisai Co., Ltd., and Teijin Pharma Co., Ltd., and speaker fees from Amgen Co., Ltd., Asahi Kasei Co., Ltd., Astellas Co., Ltd., Chugai Co., Ltd., Daiichi Sankyo Co., Ltd., Eisai Co., Ltd., Eli Lilly Co., Ltd., Ono Pharmaceutical Co., Ltd., Pfizer Co., Ltd., Taisho Co., Ltd., and UCB Japan Co., Ltd. KE is affiliated with the Department of Sports Medical Biomechanics, Osaka University Graduate School of Medicine, supported by Asahi Kasei Co., Ltd. MS supervises the Department of Gene & Stem Cell Regenerative Therapy, Osaka University Graduate School of Medicine, supported by AS medical support. YE has received research grants and/or speaker fees from Asahi Kasei Co., Ltd., Eisai Co., Ltd., Eli Lilly Co., Ltd., Ono Pharmaceutical Co., Ltd., and Taisho Co., Ltd. YE is affiliated with the Department of Sports Medical Biomechanics, Osaka University Graduate School of Medicine, supported by Asahi Kasei Co., Ltd. NO is affiliated with the Department of Musculoskeletal Regenerative Medicine, Osaka University Graduate School of Medicine, which is supported by Taisho Pharmaceutical Co., Ltd. NO is an employee of Taisho Pharmaceutical Co., Ltd. KN has received research grants from Astellas Co., Ltd. and supervises the Department of Medicine for Sports and Performing Arts, Osaka University Graduate School of Medicine, supported by Asahi Kasei Co., Ltd. These companies had no role in the study design, decision to publish, or preparation of the manuscript. TK, TN, YF, AG, TM, MH, AS, NJ, SY, TKm, and SO declare that they have no conflicts of interest.

Acknowledgments

The authors are grateful to Yukiko Eguchi, Mari Shinkawa, and Fumiko Hirayama for their contributions to this work. This study was also supported by Yuri Terao and Tomoko Yonezawa Center for Medical Research and Education, Graduate School of Medicine, Osaka University.

Data availability

The data set used or analyzed in this study is available from the corresponding author upon reasonable request.

References

- W.J. Boyle, W.S. Simonet, D.L. Lacey, Osteoclast differentiation and activation, *Nature* 423 (6937) (2003) 337–342, <https://doi.org/10.1038/nature01658>.
- J.H. Park, N.K. Lee, S.Y. Lee, Current understanding of RANK signaling in osteoclast differentiation and maturation, *Mol. Cell* 40 (10) (2017) 706–713, <https://doi.org/10.14348/molcells.2017.0225>.
- B.J. Kim, S.J. Bae, S.Y. Lee, et al., TNF- α mediates the stimulation of sclerostin expression in an estrogen-deficient condition, *Biochem. Biophys. Res. Commun.* 424 (1) (2012) 170–175, <https://doi.org/10.1016/j.bbrc.2012.06.100>.
- A. Sebastian, G.G. Loots, Transcriptional control of Sost in bone, *Bone* 96 (2017) 76–84, <https://doi.org/10.1016/j.bone.2016.10.009>.
- A. Qaseem, L.A. Hicks, I. Etzeandia-Ikobaltzeta, et al., Pharmacologic treatment of primary osteoporosis or low bone mass to prevent fractures in adults: a living clinical guideline from the American College of Physicians, *Ann. Intern. Med.* 176 (2) (2023) 224–238, <https://doi.org/10.7326/m22-1034>.
- D.M. Black, E.J. Geiger, R. Eastell, et al., Atypical femur fracture risk versus fragility fracture prevention with bisphosphonates, *N. Engl. J. Med.* 383 (8) (2020) 743–753, <https://doi.org/10.1056/NEJMoa1916525>.
- K. Pittman, Y.C. Antill, A. Goldrick, J. Goh, R.H. de Boer, Denosumab: prevention and management of hypocalcemia, osteonecrosis of the jaw and atypical fractures, *Asia Pac. J. Clin. Oncol.* 13 (4) (2017) 266–276, <https://doi.org/10.1111/ajco.12517>.
- B.C. Silva, J.P. Bilezikian, Parathyroid hormone: anabolic and catabolic actions on the skeleton, *Curr. Opin. Pharmacol.* 22 (2015) 41–50, <https://doi.org/10.1016/j.coph.2015.03.005>.
- K. Ebina, Y. Etani, T. Noguchi, K. Nakata, S. Okada, Clinical effects of teriparatide, abaloparatide, and romosozumab in postmenopausal osteoporosis, *J. Bone Miner. Metab.* (2024), <https://doi.org/10.1007/s00774-024-01536-0>.
- H. Li, Z. Xiao, L.D. Quarles, W. Li, Osteoporosis: mechanism, molecular target and current status on drug development, *Curr. Med. Chem.* 28 (8) (2021) 1489–1507, <https://doi.org/10.2174/0929867327666200330142432>.
- R.F. Mota, P.H. Cavalcanti de Araújo, M.E.R. Cezine, et al., RANKL impairs the TLR4 pathway by increasing TRAF6 and RANK interaction in macrophages, *Biomed. Res. Int.* 2022 (2022) 7740079, <https://doi.org/10.1155/2022/7740079>.
- M. Shimamura, H. Nakagami, M.K. Osako, et al., OPG/RANKL/RANK axis is a critical inflammatory signaling system in ischemic brain in mice, *Proc. Natl. Acad. Sci. U. S. A.* 111 (22) (2014) 8191–8196, <https://doi.org/10.1073/pnas.1400544111>.
- K. Maruyama, Y. Takada, N. Ray, et al., Receptor activator of NF-kappa B ligand and osteoprotegerin regulate proinflammatory cytokine production in mice, *J. Immunol.* 177 (6) (2006) 3799–3805, <https://doi.org/10.4049/jimmunol.177.6.3799>.
- M. Shimamura, H. Nakagami, H. Shimizu, et al., Development of a novel RANKL-based peptide, microglial healing peptide1-AcN (MHP1-AcN), for treatment of ischemic stroke, *Sci. Rep.* 8 (1) (2018) 17770, <https://doi.org/10.1038/s41598-018-35898-z>.
- N. Ju, M. Shimamura, H. Hayashi, et al., Preventative effects of the partial RANKL peptide MHP1-AcN in a mouse model of imiquimod-induced psoriasis, *Sci. Rep.* 9 (1) (2019) 15434, <https://doi.org/10.1038/s41598-019-51681-0>.
- N. Ju, H. Hayashi, M. Shimamura, et al., Prevention of acute lung injury by a novel CD14-inhibitory receptor activator of the NF-kappaB ligand peptide in mice, *Immunohorizons* 5 (6) (2021) 438–447, <https://doi.org/10.4049/immunohorizons.2000112>.
- C. Magis, A.M. van der Sloot, L. Serrano, C. Notredame, An improved understanding of TNFL/TNFR interactions using structure-based classifications, *Trends Biochem. Sci.* 37 (9) (2012) 353–363, <https://doi.org/10.1016/j.tibs.2012.06.002>.
- T. Noguchi, K. Ebina, M. Hirao, et al., Oxygen ultra-fine bubbles water administration prevents bone loss of glucocorticoid-induced osteoporosis in mice by suppressing osteoclast differentiation, *Osteoporos. Int.* 28 (3) (2017) 1063–1075, <https://doi.org/10.1007/s00198-016-3830-1>.
- H. Tsukazaki, J. Kikuta, T. Ao, et al., Anti-Siglec-15 antibody suppresses bone resorption by inhibiting osteoclast multinucleation without attenuating bone formation, *Bone* 152 (2021) 116095, <https://doi.org/10.1016/j.bone.2021.116095>.
- A.M. Tyagi, M.N. Mansoori, K. Srivastava, et al., Enhanced immunoprotective effects by anti-IL-17 antibody translates to improved skeletal parameters under estrogen deficiency compared with anti-RANKL and anti-TNF- α antibodies, *J. Bone Miner. Res.* 29 (9) (2014) 1981–1992, <https://doi.org/10.1002/jbmr.2228>.
- K. Kawamoto, K. Kawamoto, Preparation of thin frozen sections from nonfixed and undecalcified hard tissues using Kawamoto's film method (2020), *Methods Mol. Biol.* 2230 (2021) 259–281, https://doi.org/10.1007/978-1-0716-1028-2_15.
- T. Miura, Y. Etani, T. Noguchi, et al., Igaratimod suppresses sclerostin and receptor activator of NF- κ B ligand production via the extracellular signal-regulated kinase/early growth response protein 1/tumor necrosis factor alpha pathway in osteocytes and ameliorates disuse osteoporosis in mice, *Bone* 181 (2024) 117026, <https://doi.org/10.1016/j.bone.2024.117026>.
- K. Takami, K. Okamoto, Y. Etani, et al., Anti-NF- κ B peptide derived from nuclear acidic protein attenuates ovariectomy-induced osteoporosis in mice, *JCI Insight* 8 (22) (2023), <https://doi.org/10.1172/jci.insight.171962>.
- Y. Etani, K. Ebina, M. Hirao, et al., Combined effect of teriparatide and an anti-RANKL monoclonal antibody on bone defect regeneration in mice with glucocorticoid-induced osteoporosis, *Bone* 139 (2020) 115525, <https://doi.org/10.1016/j.bone.2020.115525>.
- D.W. Dempster, J.E. Compston, M.K. Drezner, et al., Standardized nomenclature, symbols, and units for bone histomorphometry: a 2012 update of the report of the ASBMR Histomorphometry Nomenclature Committee, *J. Bone Miner. Res.* 28 (1) (2013) 2–17, <https://doi.org/10.1002/jbmr.1805>.
- D. Jing, E. Luo, J. Cai, et al., Mechanical vibration mitigates the decrease of bone quantity and bone quality of leptin receptor-deficient Db/Db mice by promoting bone formation and inhibiting bone resorption, *J. Bone Miner. Res.* 31 (9) (2016) 1713–1724, <https://doi.org/10.1002/jbmr.2837>.
- H. Kurinami, M. Shimamura, H. Nakagami, et al., A novel therapeutic peptide as a partial agonist of RANKL in ischemic stroke, *Sci. Rep.* 6 (2016) 38062, <https://doi.org/10.1038/srep38062>.
- N. Ju, H. Hayashi, M. Shimamura, et al., Prevention of bleomycin-induced pulmonary fibrosis by a RANKL peptide in mice, *Sci. Rep.* 12 (1) (2022) 12474, <https://doi.org/10.1038/s41598-022-16843-7>.
- A. Miyama, K. Ebina, M. Hirao, et al., Effects of iguratimod on glucocorticoid-induced disorder of bone metabolism in vitro, *J. Bone Miner. Metab.* 39 (4) (2021) 639–648, <https://doi.org/10.1007/s00774-021-01206-5>.
- J. Lam, C.A. Nelson, F.P. Ross, S.L. Teitelbaum, D.H. Fremont, Crystal structure of the TRANCE/RANKL cytokine reveals determinants of receptor-ligand specificity, *J. Clin. Invest.* 108 (7) (2001) 971–979, <https://doi.org/10.1172/jci13890>.
- J. Hur, A. Ghosh, K. Kim, et al., Design of a RANK-mimetic peptide inhibitor of osteoclastogenesis with enhanced RANKL-binding affinity, *Mol. Cell* 39 (4) (2016) 316–321, <https://doi.org/10.14348/molcells.2016.2286>.

- [32] D. Huang, C. Zhao, R. Li, et al., Identification of a binding site on soluble RANKL that can be targeted to inhibit soluble RANK-RANKL interactions and treat osteoporosis, *Nat. Commun.* 13 (1) (2022) 5338, <https://doi.org/10.1038/s41467-022-33006-4>.
- [33] M. Jiang, L. Peng, K. Yang, et al., Development of small-molecules targeting receptor activator of nuclear factor- κ B ligand (RANKL)-receptor activator of nuclear factor- κ B (RANK) protein-protein interaction by structure-based virtual screening and hit optimization, *J. Med. Chem.* 62 (11) (2019) 5370–5381, <https://doi.org/10.1021/acs.jmedchem.8b02027>.
- [34] S. Theoleyre, Y. Wittrant, S.K. Tat, et al., The molecular triad OPG/RANK/RANKL: involvement in the orchestration of pathophysiological bone remodeling, *Cytokine Growth Factor Rev.* 15 (6) (2004) 457–475, <https://doi.org/10.1016/j.cytogfr.2004.06.004>.
- [35] Q. Fu, N.C. Bustamante-Gomez, H. Reyes-Pardo, et al., Reduced osteoprotegerin expression by osteocytes may contribute to rebound resorption after denosumab discontinuation, *JCI Insight* 8 (18) (2023), <https://doi.org/10.1172/jci.insight.167790>.
- [36] A.S. Kim, V.E. Taylor, A. Castro-Martinez, et al., Temporal patterns of osteoclast formation and activity following withdrawal of RANKL inhibition, *J. Bone Miner. Res.* 39 (4) (2024) 484–497, <https://doi.org/10.1093/jbmr/zjae023>.
- [37] G.J. Atkins, P. Kostakis, C. Vincent, et al., RANK expression as a cell surface marker of human osteoclast precursors in peripheral blood, bone marrow, and giant cell tumors of bone, *J. Bone Miner. Res.* 21 (9) (2006) 1339–1349, <https://doi.org/10.1359/jbmr.060604>.
- [38] S. Téletchéa, V. Stresing, S. Hervouet, et al., Novel RANK antagonists for the treatment of bone-resorptive disease: theoretical predictions and experimental validation, *J. Bone Miner. Res.* 29 (6) (2014) 1466–1477, <https://doi.org/10.1002/jbmr.2170>.
- [39] C.C. Chen, Y.T. Sun, J.J. Chen, K.T. Chiu, TNF-alpha-induced cyclooxygenase-2 expression in human lung epithelial cells: involvement of the phospholipase C-gamma 2, protein kinase C-alpha, tyrosine kinase, NF-kappa B-inducing kinase, and I-kappa B kinase 1/2 pathway, *J. Immunol.* 165 (5) (2000) 2719–2728, <https://doi.org/10.4049/jimmunol.165.5.2719>.
- [40] H.J. Park, K. Baek, J.H. Baek, H.R. Kim, TNF α increases RANKL expression via PGE $_2$ -induced activation of NFATc1, *Int. J. Mol. Sci.* 18 (3) (2017), <https://doi.org/10.3390/ijms18030495>.
- [41] R. Murali, X. Cheng, A. Berezov, et al., Disabling TNF receptor signaling by induced conformational perturbation of tryptophan-107, *Proc. Natl. Acad. Sci. U. S. A.* 102 (31) (2005) 10970–10975, <https://doi.org/10.1073/pnas.0504301102>.
- [42] J. Zeng, G.W.Z. Loi, E.N. Saipuljumri, et al., Peptide-based allosteric inhibitor targets TNFR1 conformationally active region and disables receptor-ligand signaling complex, *Proc. Natl. Acad. Sci. U. S. A.* 121 (14) (2024) e2308132121, <https://doi.org/10.1073/pnas.2308132121>.
- [43] C.H. Lo, T.M. Schaaf, B.D. Grant, et al., Noncompetitive inhibitors of TNFR1 probe conformational activation states, *Sci. Signal.* 12 (592) (2019), <https://doi.org/10.1126/scisignal.aav5637>.
- [44] C.J. Hernandez, Suppression of remodeling and bone fragility, *J. Bone Miner. Res.* 38 (3) (2023) 370–371, <https://doi.org/10.1002/jbmr.4781>.
- [45] M.S. Ominsky, B. Stouch, J. Schroeder, et al., Denosumab, a fully human RANKL antibody, reduced bone turnover markers and increased trabecular and cortical bone mass, density, and strength in ovariectomized cynomolgus monkeys, *Bone* 49 (2) (2011) 162–173, <https://doi.org/10.1016/j.bone.2011.04.001>.